JACS
JOURNAL OF THE AMERICAN CHEMICAL SOCIETY
Article
pubs.acs.org/JACS

Surface Fluorination of Reactive Battery Anode Materials for Enhanced Stability

Jie Zhao,[†,⊥] Lei Liao,[†,⊥] Feifei Shi,[†] Ting Lei,[‡] Guangxu Chen,[†] Allen Pei,[†] Jie Sun,[†] Kai Yan,[†] Guangmin Zhou,[†] Jin Xie,[†] Chong Liu,[†] Yuzhang Li,[†] Zheng Liang,[†] Zhenan Bao,[‡] and Yi Cui*[,†,§]

[†]Department of Materials Science and Engineering, Stanford University, Stanford, California 94305, United States
[‡]Department of Chemical Engineering, Stanford University, Stanford, California 94305, United States
[§]Stanford Institute for Materials and Energy Sciences, SLAC National Accelerator Laboratory, 2575 Sand Hill Road, Menlo Park, California 94025, United States

Supporting Information

ABSTRACT: Significant increases in the energy density of batteries must be achieved by exploring new materials and cell configurations. Lithium metal and lithiated silicon are two promising high-capacity anode materials. Unfortunately, both of these anodes require a reliable passivating layer to survive the serious environmental corrosion during handling and cycling. Here we developed a surface fluorination process to form a homogeneous and dense LiF coating on reactive anode materials, with *in situ* generated fluorine gas, by using a fluoropolymer, CYTOP, as the precursor. The process is effectively a "reaction in the beaker", avoiding direct handling of highly toxic fluorine gas. For lithium metal, this LiF coating serves as a chemically stable and mechanically strong interphase, which minimizes the corrosion reaction with carbonate electrolytes and suppresses dendrite formation, enabling dendrite-free and stable cycling over 300 cycles with current densities up to 5 mA/cm^2. Lithiated silicon can serve as either a pre-lithiation additive for existing lithium-ion batteries or a replacement for lithium metal in Li−O_2 and Li−S batteries. However, lithiated silicon reacts vigorously with the standard slurry solvent *N*-methyl-2-pyrrolidinone (NMP), indicating it is not compatible with the real battery fabrication process. With the protection of crystalline and dense LiF coating, Li_xSi can be processed in anhydrous NMP with a high capacity of 2504 mAh/g. With low solubility of LiF in water, this protection layer also allows Li_xSi to be stable in humid air (~40% relative humidity). Therefore, this facile surface fluorination process brings huge benefit to both the existing lithium-ion batteries and next-generation lithium metal batteries.

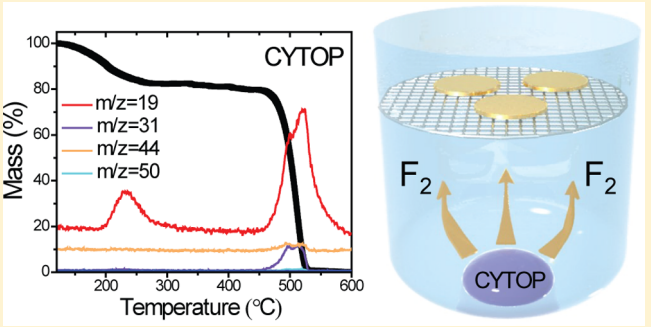

INTRODUCTION

Commercial lithium-ion batteries (LIBs) based on graphite anodes and lithium metal oxide cathodes are rapidly falling behind the high-energy storage demands of portable electronics and electric vehicles.[1−3] For the next generation of LIB technology, significant increases in energy density must be achieved by developing new battery chemistries, based on different storage mechanisms at the material level, and different configurations at the cell level.[4,5] Among them, plating- and stripping-type lithium metal anodes,[6,7] alloy-type Si, Sn anodes,[8,9] oxygen redox in transition metal oxide cathodes,[10,11] and S (Li−S batteries, lithiated Si−S batteries)[12,13] and O_2 (Li−air batteries, lithiated Si−air batteries)[14,15] cathodes have attracted extensive interest and demonstrated great promise.

However, Li-containing high-capacity anodes, including Li metal and pre-lithiated Si, require reliable passivating interfacial layer to survive the serious environmental corrosion during handling and cycling.[16,17] Due to its high chemical reactivity, Li metal spontaneously reacts with organic electrolytes to form a layer of solid electrolyte interphase (SEI) which is mechanically unstable during Li stripping/plating.[6,18,19] SEI instability coupled with dramatic volume changes during cycling can expose pristine Li metal surfaces, leading to locally enhanced Li^+ ion flux and dendrite formation, which gives rise to potential safety hazards such as internal short circuits and thermal runaway.[20,21] Recently, three-dimensional (3D) Li hosts including graphene oxide and nanofiber were demonstrated to minimize the volume changes although stable SEI is yet to be demonstrated.[22,23] Moreover, the SEI on Li metal is heterogeneous in chemical compositions and physical structures, resulting in non-uniform Li deposition which aggravates the growth of dendrites.[24,25] Therefore, the formation of an electrode/electrolyte interphase with high stability and uniformity is essential to ensure the long cycle life and safety of Li metal batteries. Recently, Cu current collectors were modified with carbon nanospheres,[26] boron nitride, and graphene as stable interfacial layers.[27] Ceramic-type protection

Received: May 22, 2017
Published: July 26, 2017

DOI: 10.1021/jacs.7b05251
J. Am. Chem. Soc. XXXX, XXX, XXX−XXX

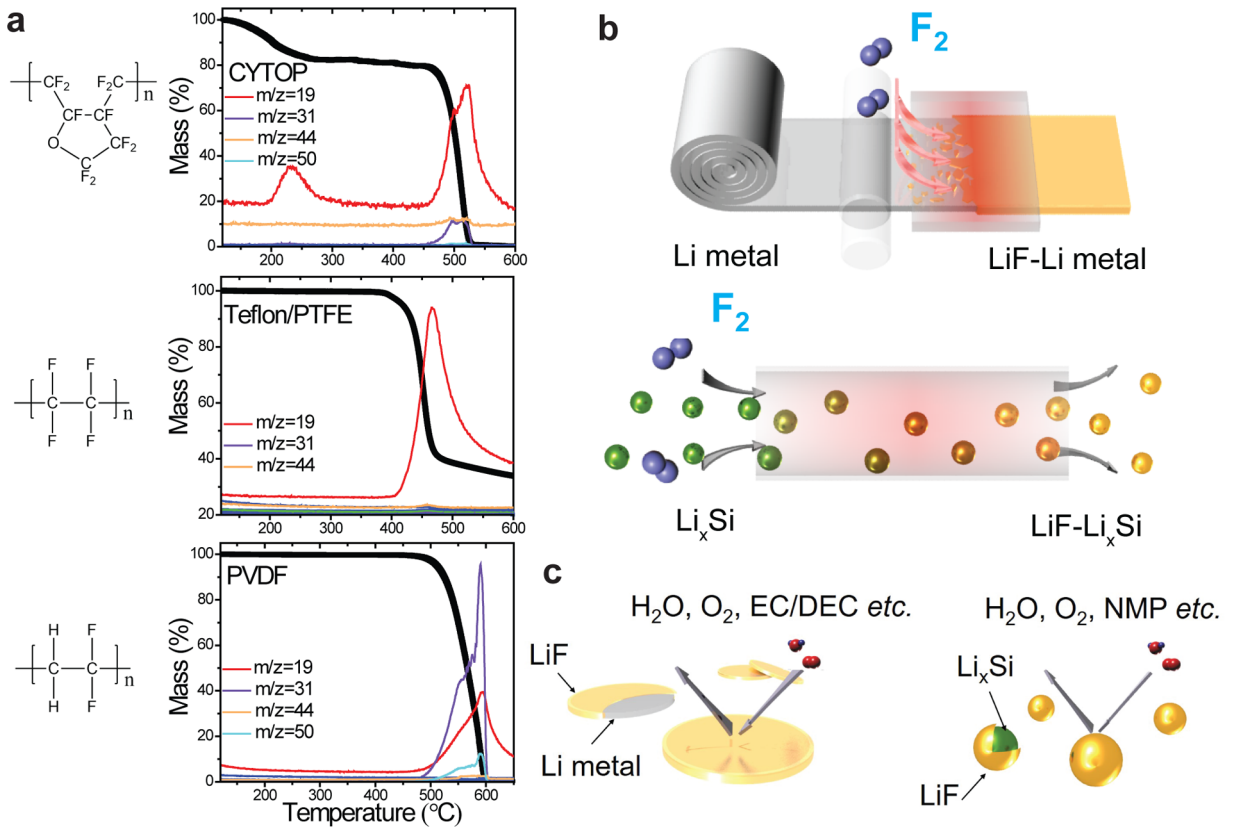

Figure 1. Surface fluorination of lithium metal and pre-lithiated silicon anodes. (a) Thermogravimetric analysis–mass spectrometry (TGA-MS) of three fluoropolymers (CYTOP, Teflon/PTFE, and PVDF) under inert atmosphere shows only CYTOP releases F_2 at temperature lower than 250 °C. (b) A schematic illustrates that the fluoropolymer, CYTOP, gradually decomposes and releases pure F_2 gas upon heating, which reacts with Li metal or Li_xSi NPs to form a uniform and compact LiF coating. (c) With ultralow solubility in both water and organic solvents, LiF coating on Li metal anodes suppresses corrosion reactions with carbonate electrolytes and atmosphere contaminants. For pre-lithiated anode materials such as Li_xSi, LiF coating improves their compatibility with industrial fabrication process, particularly the processability in the regular slurry solvent of NMP.

film[28,29] and oxide films by atomic layer deposition[30,31] were directly grown on Li metal. Unfortunately, the stability of these coatings at the working potential of anodes needs further improvement. With exceptional chemical stability in highly reducing environment and extremely low solubility in electrolytes ($<4 \times 10^{-4}$ mol/L in diethyl carbonate (DEC)),[32] LiF is a promising interfacial material able to suppress the corrosion reaction with organic electrolytes. Moreover, LiF is mechanically strong enough (Shear modulus of 55.1 GPa) to suppress and withstand breakthrough by Li dendrites.[6,33] Previously, electrolyte additives, including hydrogen fluoride (HF),[34] fluoroethylene carbonate (FEC)[35−37] and LiF NPs,[38,39] have been utilized to incorporate LiF into the SEI. The additive-reinforced SEI increases the cycle life at relatively low current densities (<0.5 mA/cm^2), but dendrite formation was still observed, especially at high current densities. During the formation of LiF layers, side reactions between Li metal and electrolytes are inevitable, resulting in heterogeneous SEI layers.[38] Moreover, loosely connected LiF domains and the porous nature of the SEI layer cannot prevent the penetration of corrosive carbonate electrolytes. Formation of a compact and homogeneous LiF passivation layer on Li metal before cell assembly is therefore highly desirable.

With low solubility in both water (0.134 g/100 mL at 25 °C) and organic solvents,[32,40] LiF coating is also applicable to pre-lithiated anodes like Li_xSi to improve compatibility with industrial electrode fabrication processes. The common issue for anode materials is the irreversible consumption of Li due to the formation of SEI during the first cycle.[41] Because of its high capacity and low potential, Li_xSi has been used as a pre-lithiation additive to increase the first cycle Coulombic efficiency (CE) of various anode materials.[42,43] Pre-lithiated Si anodes may also serve as the replacement for the dendrite-forming Li metal in Li−O_2 and Li−S batteries.[12,15] However, pre-lithiated anodes are neither stable in air nor in polar slurry solvents like NMP.[42,44] Despite being stable in dry air, Li_2O-coated Li_xSi NPs react rapidly in humid air since Li_2O reacts violently with water, suggesting LiF as a better anticorrosion layer. Previously, Li_xSi NPs modified by 1-fluorodecane was coated with an artificial-SEI layer consisting of LiF and lithium decylcarbonate.[45] However, these particles maintain their capacity only in air with low humidity levels (<10% relative humidity (RH)), and their stability in NMP is not possible. The LiF formed at room temperature with this method is amorphous, and the coating consists of side products resulting in a less dense coating which is unable to prevent the penetration of water and NMP. Therefore, a pure and crystalline LiF anticorrosion layer is highly desired for reactive Li-containing anodes.

Here we develop a convenient surface fluorination reaction using a fluoropolymer, CYTOP, as a solid and non-toxic fluorine source.[46] Among common fluoropolymers, CYTOP decomposes and gradually releases pure fluorine gas at relatively low temperature, which reacts with Li metal or pre-

DOI: 10.1021/jacs.7b05251
J. Am. Chem. Soc. XXXX, XXX, XXX−XXX

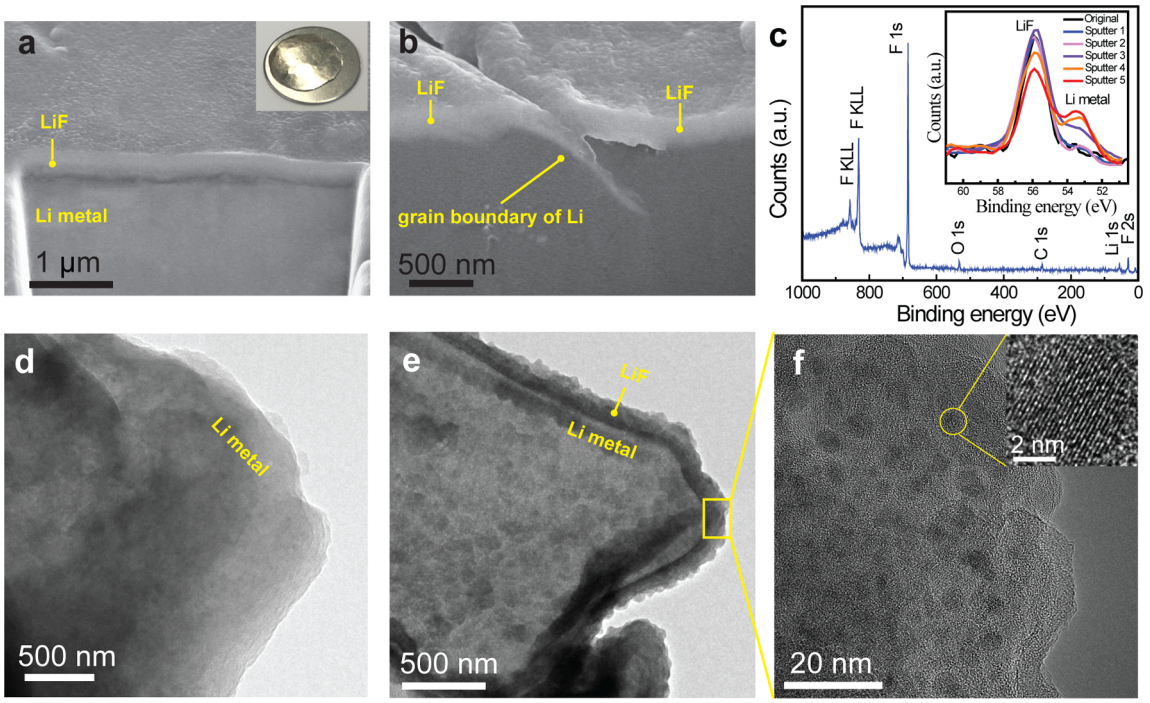

Figure 2. Characterization of LiF-coated Li metal. (a) Cross-sectional focused ion beam (FIB)-scanning electron microscope (SEM) image of LiF-coated Li metal. The inset is the photograph of LiF-coated Li metal showing a shiny golden color. (b) FIB-SEM image indicates that LiF layers on different grains merge together to form a continuous coating fully covering grain boundary of Li metal. (c) XPS spectrum of LiF-coated Li metal. The sputtering depth profile of Li 1s spectra is shown in the inset. TEM images of a Li metal particle (d) before and (e) after LiF coating. (f) A magnified TEM image shows a dense coating layer composed of ultrafine crystallites in the range of 5−10 nm. Inset: High-resolution TEM image reveals the (111) lattice plane of a LiF nanocrystal with plane spacing of 0.234 nm.

lithiated Si anodes to form a homogeneous and compact LiF coating (Figure 1 and Figure S1). With exceptional chemical stability in highly reducing environment, extremely low solubility in electrolytes, and strong mechanical property, LiF coating minimizes the corrosion reaction between Li metal and carbonate electrolytes and suppresses dendrite formation (Figure 1c). Therefore, LiF-coated Li metal anodes exhibit dendrite-free and stable cycling over 300 cycles at current densities of 1 mA/cm^2 and 5 mA/cm^2. With crystalline and dense LiF coating, Li_xSi NPs are processable in NMP with a high capacity of 2504 mAh/g. They also exhibit excellent stability in humid air (~40% RH) with 85.9% capacity retention after 1 day. During the battery operation, the decomposition of electrolytes is minimized with the protection of inert LiF coating, thereby enabling high CEs of LiF-Li_xSi NPs during long-term cycling (average CE of 99.92% from the third cycle to 650th cycles). Accordingly, LiF serves as a general passivation coating for highly reactive Li-containing anode materials.

RESULTS AND DISCUSSION

Fabrication and Characterization of LiF-Coated Li Metal. Among three common fluoropolymers including CYTOP, Teflon, and polyvinylidene fluoride (PVDF) investigated in our study, only CYTOP releases pure F_2 gas at temperature lower than 250 °C, by tracing the signals of $C_xH_yF_z$ (x, y, z = 0, 1, 2, ...) fragments with mass-to-charge ratio less than 138 based on the thermogravimetric analysis−mass spectrometry (TGA-MS) under inert atmosphere (Figure 1a and Figure S2). In contrast, other fluoropolymers decompose at higher temperature and release hydrofluorocarbons, which will contribute defects and impurities in the LiF coating, facilitating the growth of Li dendrites. Therefore, CYTOP is selected as solid fluorination precursor to generate pure F_2 gas by heating at 350 °C. The temperature of surface fluorination reaction with Li metal is kept at 175 °C and held for 12 h to ensure the formation of a homogeneous and crystalline LiF coating layer (Figure S1). As the inset of Figure 2a illustrates, Li metal remains shiny and turns slightly golden color after the LiF coating. The morphology and thickness of the LiF coating are characterized by focused ion beam−scanning electron microscopy (FIB-SEM). The LiF coating (Figure 2a) is continuous and uniform with a thickness of ~380 nm. Li metal naturally contains a rough surface with grain boundaries and cracks. Figure 2b shows that LiF layers on different grains merge together to form a continuous coating covering grain boundary of Li metal. X-ray photoelectron spectroscopy (XPS) reveals the major component as LiF with extremely low percentage of oxygen and carbon contaminants (<4%, Figure 2c). The XPS spectra before and after the first sputtering both show a single F1s peak at 685 eV (Figure S3) and a single Li 1s peak at 56 eV, indicating the high purity and robustness of the LiF coating. With further sputtering, the Li 1s peak of Li metal is observed while the intensity of the peak corresponding to LiF decreases gradually, confirming the formation of a pure LiF coating on Li metal foil (inset of Figure 2c). Transmission electron microscopy (TEM) was utilized to further characterize the morphology and composition of the coating. The TEM sample of a bare Li particle was prepared by dipping a TEM grid into molten Li. The surface of the Li particle is initially clean and smooth (Figure 2d). To prepare the protection layer, the Li-coated TEM grid was placed in the fluorination reactor and heated under the same condition. The TEM image (Figure 2e) indicates the Li particle is wrapped in a uniform coating of

DOI: 10.1021/jacs.7b05251
J. Am. Chem. Soc. XXXX, XXX, XXX−XXX

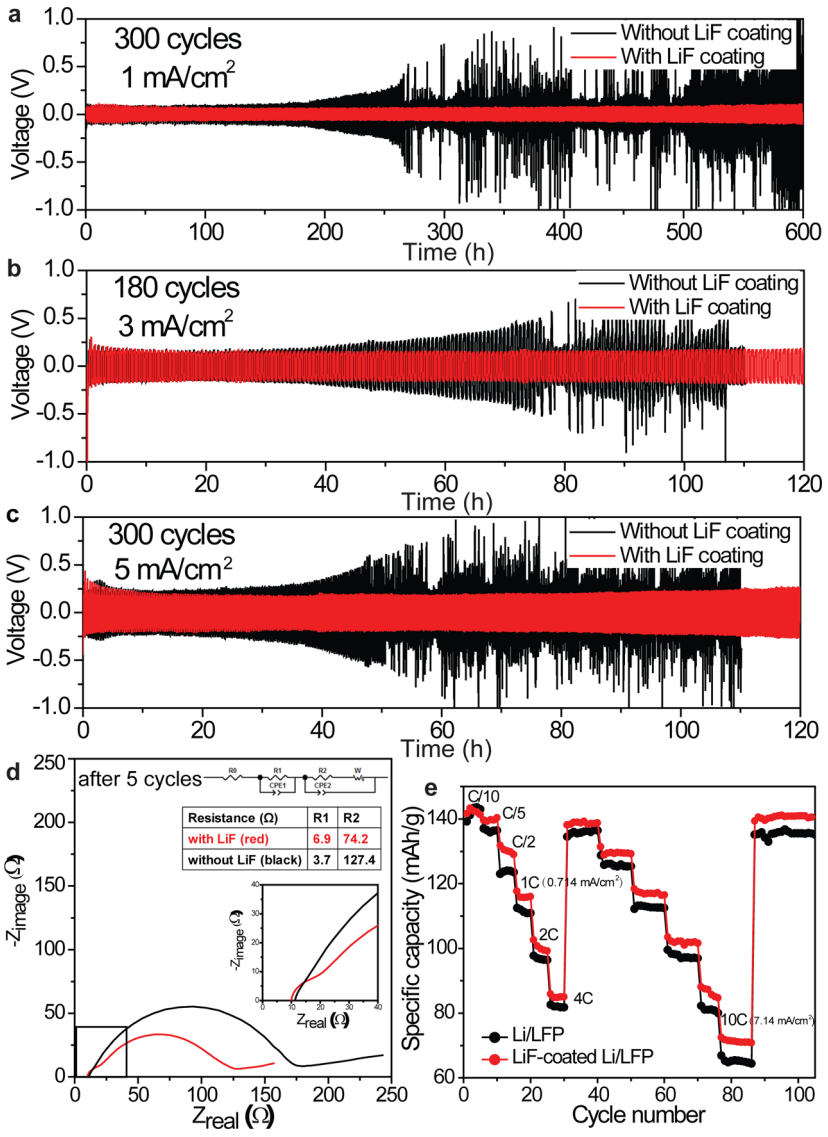

Figure 3. Electrochemical characterization of LiF-coated Li metal. A comparison of the cycling stability of the symmetric LiF-coated Li metal (red) and bare Li metal (black) cells with carbonate electrolytes at a current density of (a) 1 mA/cm^2, (b) 3 mA/cm^2, and (c) 5 mA/cm^2, respectively. (d) Nyquist plot of the impedance spectra of the symmetric LiF-coated Li metal and bare Li metal cells after five cycles at a current density of 1 mA/cm^2. (e) Rate capability of the LiF-coated Li metal/$LiFePO_4$ (LFP) and the bare Li metal/LFP cells at various rates from 0.1C to 10C. The capacity and rate are both based on the mass of LFP in the cathodes (1C = 0.17 A/g of LFP). Since the mass loading of the LFP cathode is 6 mg/cm^2, the current density of the cell is 0.714 mA/cm^2 for 1C and 7.14 mA/cm^2 for 10C.

~100 nm thick. The thickness increases from 25 to 100 nm by extending the reaction time from 1 h to 6 h (Figure S4). The high resolution TEM image shows that the dense LiF coating layer is composed of ultrafine crystallites with sizes ranging from 5 nm to 10 nm (Figure 2f). Two sets of lattices with plane spacings of 0.234 nm and 0.204 nm are observed, corresponding to LiF (111) and (200) lattice planes, respectively (inset of Figure 2f and Figure S5).

Electrochemical Characterization of LiF-Coated Li Metal. To investigate the electrochemical performance, two-electrode symmetric cells were assembled with carbonate electrolyte (1 M lithium hexafluorophosphate ($LiPF_6$) in 1:1 ethylene carbonate (EC)/DEC). The LiF coating is expected to be an improved protection layer, by minimizing the consumption of organic electrolytes. To illustrate the stabilizing effect, a limited electrolyte of only 20 μL was added into symmetric cells. The bare Li metal symmetric cell (20 μL carbonate electrolyte) succumbs to substantial voltage fluctuation after 140 cycles at a current density of 1 mA/cm^2, which may be attributed to the drying up of organic electrolytes and dendrite-induced short-circuit (Figure 3a). With 60 μL of carbonate electrolyte, the bare Li metal cell succumbs to substantial voltage fluctuation after 240 cycles, which confirms that the drying up of carbonate electrolytes is the major reason for the death of the Li metal cells (Figure S6). In contrast, the LiF-coated Li metal symmetric cell with only 20 μL of carbonate electrolyte outperformed the bare Li metal, exhibiting a long-term cycling of more than 300 cycles at a current density of 1 mA/cm^2 (Figure 3a). For the first several cycles, two symmetric cells exhibit comparable overpotential of 50 mV versus Li^+/Li. After 130 cycles, the overpotential of the bare Li metal cell increases considerably (>250 mV), while the overpotential of the LiF-coated Li metal cell is stable with a minor increase (60 mV). Electrochemical impedance spectros-

DOI: 10.1021/jacs.7b05251
J. Am. Chem. Soc. XXXX, XXX, XXX−XXX

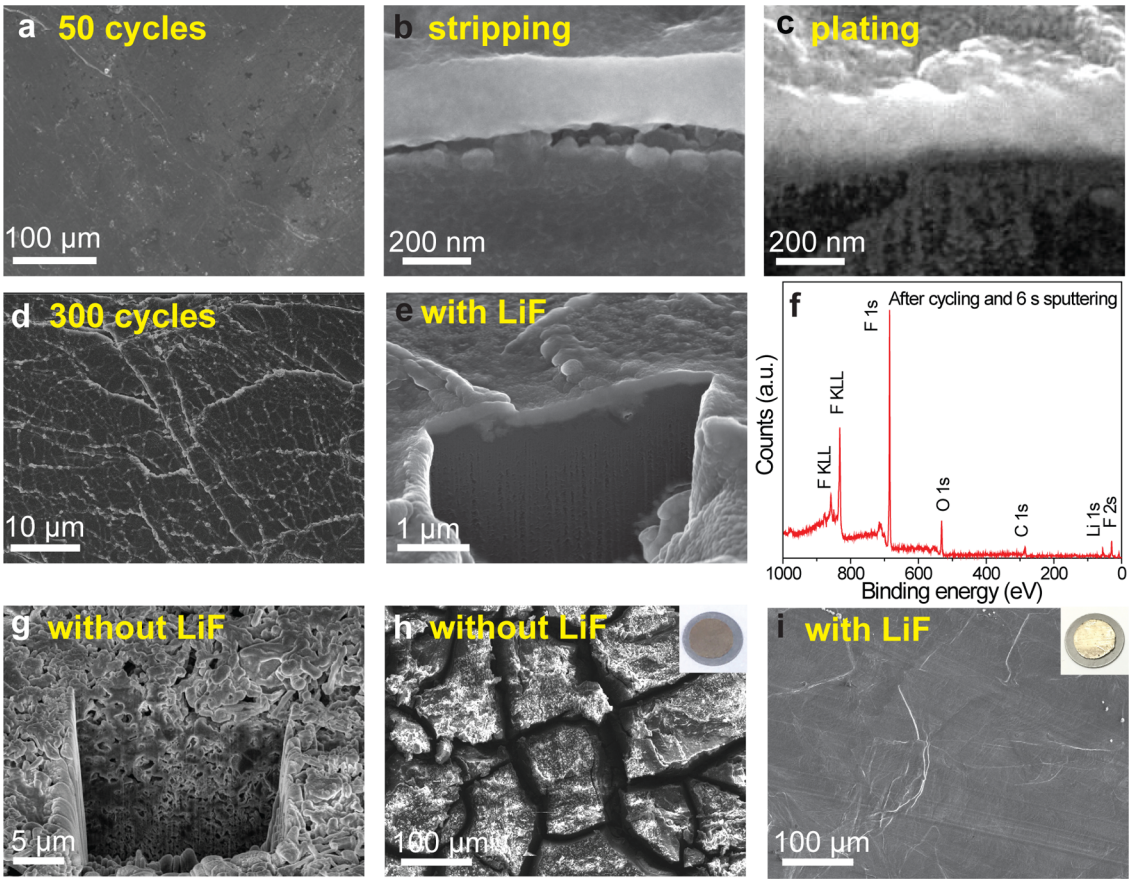

Figure 4. Characterization of Li electrodes after cycling. (a) SEM image of LiF-coated Li metal after 50 cycles of stripping/plating in the symmetric cell with the electrolyte of EC/DEC. Cross-sectional FIB-SEM images of two LiF-coated Li metal electrodes cycled in the symmetric cell for 50 times. The electrodes correspond to the (b) stripped state and (c) plated state. The (d) FIB-SEM image and (e) cross-sectional FIB-SEM image of LiF-coated Li metal after 300 cycles of stripping/plating in EC/DEC. (f) XPS spectrum of the LiF-coated Li metal after 300 cycles. Six-second ion gun sputtering is performed to remove the Li salts residue. (g) Cross-sectional FIB-SEM image of the bare Li metal electrode cycled in the symmetric cell for 300 cycles. SEM images of (h) uncoated and (i) coated Li metal soaked in DEC for 6 h. The insets are the corresponding photographs.

copy (EIS) was performed on the symmetric cells at different stages. The EIS spectrum of LiF-coated Li metal cell after the first cycle shows a slight increase in the overall impedance because of the fluorination treatment (Figure S7). The EIS spectrum of LiF-coated Li metal cell after five cycles exhibits two obvious semicircles (inset of Figure 3d). The smaller one at high frequency corresponds to the LiF/Li interface. The equivalent circuits show a larger R_1 (6.9 Ω) for the LiF-coated Li metal cell, indicating the LiF coating is thicker than the compact part of SEI formed in the bare Li cell.[47] The smaller overall impedance of the LiF-coated Li metal cell might be attributed to the chemical stability of the LiF coating, which minimizes electrolyte decomposition and side reactions on the electrolyte/electrode interface. The XPS analysis and sputtering depth profile show that the SEI formed on the LiF-coated Li metal after 300 cycles can be majorly removed by just 6 s sputtering (Figure S8). The SEI layer formed on the bare Li metal after just 50 cycles cannot be removed even after 4 min sputtering (Figure S9). It indicates decomposition of organic electrolytes is significantly minimized and the SEI layer on the LiF coating is indeed thin.

The difference in cycling stability becomes increasingly pronounced at higher current densities. The striping/plating overpotentials for LiF-coated Li metal cells remain stable within 180 cycles and 300 cycles at current densities of 3 mA/cm^2 and 5 mA/cm^2 for Li plating/stripping capacity of 1 mAh/cm^2, while the overpotential of bare Li metal cells increases considerably during cycling (Figure 3b,c). The bare Li metal cells exhibit an irregularly fluctuating voltage profile after 110 cycles at a current density of 3 mA/cm^2 and after 125 cycles at 5 mA/cm^2. Since the LiF coating is composed of ultrafine crystallites in the range of 5 to 10 nm, fast ion transport may be realized via the grain boundaries, which enables the excellent cycling performance at high current densities. The excellent performance of the LiF-coated Li metal in symmetric cells makes it possible to be used in full cells. First, the LiF-coated Li metal is paired with $LiFePO_4$ (LFP) cathode (LFP:Super P:PVDF = 70:20:10 by weight). The rate capability of the LiF-coated Li metal/LFP and the Li metal/LFP cells was tested at various rates from C/10 to 10C (1C = 0.17 A/g of LFP, Figure 3e). Since the mass loading of the LFP cathode is 6 mg/cm^2, the current density of the cell is 0.714 mA/cm^2 for 1C and 7.14 mA/cm^2 for 10C. At the rate of C/10, the capacities of LFP in two cells are similar. LFP in the LiF-coated Li metal/LFP cell exhibits higher capacity especially at a high rate of 10C, which is ascribed to the much stable LiF-coated Li metal counter electrode with better rate capability (stable voltage profiles with small hysteresis at different current densities). Consistently, the LiF-coated Li metal/$Li_4Ti_5O_{12}$ (LTO) cell exhibited higher capacity, and CE cycled at the rate of 1C, compared with bare

DOI: 10.1021/jacs.7b05251
J. Am. Chem. Soc. XXXX, XXX, XXX−XXX

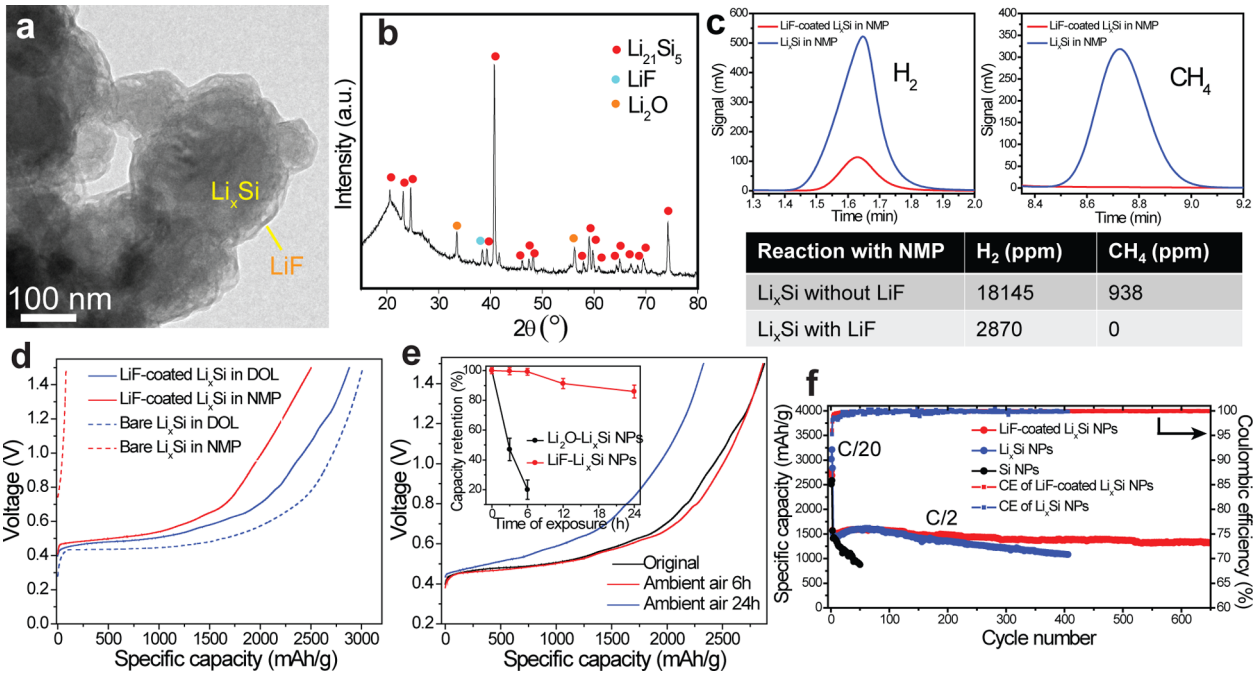

Reaction with NMP	H_2 (ppm)	CH_4 (ppm)
Li_xSi without LiF	18145	938
Li_xSi with LiF	2870	0

Figure 5. Characterization and stability of LiF-coated Li$_x$Si NPs. (a) TEM image and (b) XRD pattern of LiF-coated Li$_x$Si NPs. (c) The amount of gas released for coated (red) and uncoated (blue) Li$_x$Si NPs reacted with NMP measured by gas chromatography. (d) First-cycle delithiation capacities of LiF-coated Li$_x$Si NPs (solid line) and bare Li$_x$Si NPs (dashed line) using different solvents to form the slurry. (e) The extraction capacities of LiF-coated Li$_x$Si NPs exposed to ambient air (~40% RH) with varying durations. The inset shows the trend of capacity decay of LiF-coated Li$_x$Si NPs (red) and Li$_2$O-coated Li$_x$Si NPs (black) with varying durations. (f) Cycling performance of LiF-coated Li$_x$Si NPs (red), bare Li$_x$Si NPs (blue), and Si NPs control cell (black) at C/20 for the first several cycles and C/2 for the following cycles (1C = 4.2 A/g, and the capacity is based on the mass of Si in the electrodes). The Coulombic efficiency is plotted on the secondary *y*-axis (LiF-coated Li$_x$Si NPs, red, and bare Li$_x$Si NPs, blue).

Li metal/LTO cell (Figure S10a). The protection effect of the LiF coating on Li metal electrodes was further examined in the Li/polysulfides cells. To better show the stabilizing effect of the LiF coating, the common electrolytes additive, $LiNO_3$, is avoided. The Li/polysulfides and LiF-coated Li/polysulfides cells were tested at C/10 for first two cycles and C/5 for later cycles (Figure S10b, 1C = 1.67 A/g of S). The conformal and dense LiF coating effectively improves the cycling performance with high capacity retention above 1000 mAh/g after 100 cycles. Moreover, the LiF protection layer stabilizes the Li metal interface and alleviates lithium polysulfide shuttling, which in turn improves the average CE from ~95.7% (blue) to ~99.0% (red).

Morphology of the Li Electrodes after Cycling. The morphology of the LiF-coated Li metal electrodes was studied after 50 cycles of stripping/plating in symmetric cells. The SEM image confirms the surface remains essentially flat with no obvious dendrites (Figure 4a). The low magnification SEM image is intentionally used to remove selection bias. FIB-SEM was further utilized to study the morphology of LiF-coated Li metal electrodes after cycling. The surface texture of LiF-coated Li metal was better observed at a tilt angle of 52°, revealing boundaries and some wrinkles instead of any dendrites (Figure S11a,b). Two LiF-coated Li metal electrodes from a symmetric cell were both cross-sectioned with a Ga^+ ion beam and observed with an electron beam. A clear gap is observed beneath the protective layer for the electrode at the stripped state (Figure 4b). For the electrode at the plated state, no empty space is observed, and the LiF coating is in intimate contact with the Li metal (Figure 4c). Since Li plating only occurs where electrons meet Li ions, the electronically insulating LiF coating was rendered unfavorable for Li nucleation. Therefore, it is favorable for Li to be plated back into the empty region beneath the protective layer formed during Li stripping. Accordingly, uneven Li deposition and dendrite growth are suppressed. With 6 h fluorination treatment of the Li metal foil, the thickness of the LiF coating is 100−150 nm, and the LiF coating does not fully cover the Li metal foil. Li metal tends to be plated on the highly conductive exposed Li metal surface, accelerating the dendrites formation, which also validates the excellent protective advantage of the LiF coating (Figure S11c,d). As shown in the FIB-SEM image (Figure 4d), there are still no dendrites even after 300 cycles for the LiF-coated Li metal electrodes with 12 h surface fluorination treatment. The LiF-coated Li metal electrode remains flat in general, but boundaries and wrinkles become obvious. The cross-sectional FIB-SEM image further confirms the robustness of LiF coating, which is durable for at least 300 cycles (Figure 4e). XPS survey indicates LiF remains the major component of the surface even after 300 cycles (Figure 4f and Figure S8). The XPS spectrum of F 1s shows two main peaks at 687.5 eV and 685 eV, corresponding to $LiPF_6$ and LiF, respectively. After 6 s sputtering, the unwashed Li salts are removed, and the XPS shows a single F 1s peak at 685 eV, indicating that the composition of the coating is maintained. With LiF coating, Li metal underneath remains dense after long-term cycling. On the contrary, the bare Li metal is thoroughly corroded by the organic electrolyte to form porous structures with massive dendrites after cycling under the same condition (Figure 4g). For Li metal covered with ball-milled LiF NPs, massive dendrites form after only 10 cycles (Figure S11e,f). The loosely connected LiF NPs cannot prevent the

DOI: 10.1021/jacs.7b05251
J. Am. Chem. Soc. XXXX, XXX, XXX−XXX

penetration of corrosive carbonate electrolytes, resulting in porous and non-uniform SEI, which accelerates the dendrites formation.

There are several critical factors for the dendrite-free and long-term cycling performance of our LiF-coated Li metal cells. (1) The compact and uniform LiF coating, with low solubility in electrolytes, serves as a protection layer to prevent the penetration of organic electrolyte and subsequent corrosion of the underlying Li metal. After soaking in DEC for 6 h, the color of the bare Li metal changes to brown (inset of Figure 4h). Cracks form coming from the rapid corrosion reaction between Li metal and DEC (Figure 4h), producing $CH_3CH_2OCO_2Li$ and CH_3CH_2OLi (Figure S12). LiF-coated Li metal soaked in DEC for the same time remains lustrous and flat, indicating the LiF coating effectively suppresses the side reactions between Li and corrosive electrolytes (Figure 4i). (2) The second advantage of the LiF coating is its homogeneity in chemical composition and physical structure, leading to uniform Li deposition and consequently suppressed dendrite formation. Our LiF coating is superior compared with LiF formed from F-containing additives, which consists of LiF mixed with a variety of side-products. Both XPS spectrum of C 1s and depth profiles of Li 1s (Figure S13) indicate the existence of complex species, such as LiF, Li_2O, and $ROCO_2Li$, on the surface of Li metal cycled in electrolytes of 1.0 M $LiPF_6$ in 1:1 EC/DEC with 10 vol% FEC for only one cycle. (3) LiF, with shear modulus 10 times higher than that of Li, is mechanically strong enough to suppress the growth of Li dendrites.[6,35] Aside from its contributions to cell performance, the LiF coating improves the stability of Li electrodes in humid air, which is particularly important from a processing perspective (Figure S14).

Characterization and Stability of LiF-Coated Li_xSi NPs. Li_xSi NPs were prepared by heating a stoichiometric mixture of Li metal and Si NPs under mechanical stirring in argon atmosphere. Like the formation of LiF on Li metal, a crystalline LiF coating is uniformly grown on Li_xSi NPs via a similar process. To ensure crystalline quality, the temperature for surface fluorination reaction is kept at 350 °C. The TEM image in Figure 5a indicates a uniform and continuous coating with a thickness of 20 nm. Before LiF coating, the synthesized NPs consist of crystalline $Li_{21}Si_5$ (PDF# 00-018-747) and intrinsic Li_2O (PDF# 04-001-8930, Figure S15a). After coating, a new peak at 38.7° is indexed as LiF (PDF# 00-004-0857), confirming the crystalline nature of the coating (Figure 5b). Consistently, the XPS reveals a single F 1s peak at 685 eV (Figure S16). Furthermore, the considerably screened Si 1s peak around 100 eV provides evidence for the conformal nature of LiF coating. The reaction between Li_xSi and NMP as well as the improved stability after LiF coating was studied by gas chromatography (GC, Figure 5c). After soaking in NMP for 6 h, 20 mg of Li_xSi NPs reacted with NMP vigorously to release 18145 ppm of H_2 and 938 ppm of CH_4. The detailed reaction mechanism is shown in Figure S17. TEM imaging indicates the NPs are totally corroded after soaked in NMP (Figure S18b). XRD confirms the formation of Li_2CO_3 after the reaction (Figure S15b). With LiF coating, the reaction with NMP is considerably suppressed. The surface of NPs is clean, and the core−shell structure remains almost unchanged (Figure S18c). The GC signal of H_2 decreases to only 15% of that of uncoated Li_xSi, and no signal of CH_4 is detected. To confirm the stability of LiF-Li_xSi NPs in the slurry, LiF-Li_xSi NPs were mixed with Super P and PVDF (65:20:15 by weight) in 1,3-dioxolane (DOL) or NMP to form a slurry which was then drop cast on copper foil. Previously, we found that bare Li_xSi NPs are stable in DOL but reacts vigorously with NMP to leave almost no extraction capacity (dashed lines, Figure 5d).[42] Consistently, LiF-Li_xSi NPs shows a high capacity of 2879 mAh/g using DOL as the slurry solvent, based on the mass of Si in the cell. Replacing DOL with NMP, only a small fraction of capacity (~13%) is sacrificed (Figure 5d). In contrast to our previous work, Li_xSi directly reacts with F_2 gas at high temperature, forming a dense and crystalline LiF coating which imparts improved stability in NMP.[45] Because of the limited solubility of LiF in water, LiF further improves the stability of Li_xSi NPs in humid air. After being stored in humid air (~40% RH) for 1 day, the capacity of LiF-Li_xSi NPs is 2328.9 mAh/g, showing a high capacity retention of 85.9% (Figure 5e). The capacity decay is slow, compared with Li_2O−Li_xSi NPs as shown in the inset of Figure 5e. Without LiF coating, Li_xSi primarily reacts with O_2 and H_2O to form LiOH (PDF# 00-032-0564) after exposed to humid air (Figure S19). In contrast, no peaks belonging to LiOH are present in the XRD pattern of LiF-Li_xSi NPs exposed to the same condition. The crystalline and dense LiF coating eliminates the side reactions in both NMP and humid air, increasing the feasibility of incorporating LiF-Li_xSi NPs in the commercial electrodes fabrication process.

The cycling stability of LiF-Li_xSi NPs was tested at C/20 for the first two cycles and C/2 for the following cycles (1C = 4.2 A/g of Si, Figure 5f). Compared with Si NPs and bare Li_xSi NPs, LiF-Li_xSi NPs exhibit improved cycling performance with 13% capacity decay after 650 cycles. Li_xSi NPs are already in their fully expanded state, which contributes to the excellent cyclability. Void space is created during the delithiation process, which accommodates further volume expansion of subsequent lithiation process. Therefore, each particle does not squeeze against each other to damage the structure of the whole electrode during cycling (Figure S20a). The average CE of bare Li_xSi NPs (from the fourth cycle to the 400th cycle) is 99.79%, lower than the value of the LiF-coated Li_xSi NPs (99.92%, from the third cycle to the 650th cycle). With exceptional chemical stability, the LiF coating effectively minimizes electrolyte decomposition and side reactions on the electrolyte/electrode interface during cycling, which contributes to the high CE. TEM image confirms the core−shell structure remains after cycling, while the thickness of the coating slightly increases to 30 nm (Figure S20b). Because of the low potential and high capacity, LiF-Li_xSi NPs are sufficiently reactive as a pre-lithiation additive to compensate for the initial capacity loss of graphite. Processed in DOL and NMP, the first cycle CE of graphite increases from 86% to 102% and 99.5%, respectively, after addition of 4% LiF-Li_xSi NPs (Figure S21). This result also validates the improved stability in NMP with the LiF coating.

CONCLUSIONS

In conclusion, we have developed a facile surface fluorination process to form homogeneous and dense LiF coating on high-capacity Li-containing anode materials. CYTOP is identified as an ideal fluoropolymer precursor that decomposes and releases pure fluorine gas at relatively low temperature, avoiding handling highly toxic fluorine gas directly. The LiF coating serves as a chemically stable and mechanically strong interfacial layer for Li metal anodes by minimizing corrosion reactions with carbonate electrolytes and suppressing the dendrite formation. As such, LiF-coated Li metal cells exhibit dendrite-free and stable cycling over 300 cycles in carbonate electrolytes

DOI: 10.1021/jacs.7b05251
J. Am. Chem. Soc. XXXX, XXX, XXX−XXX

at current densities of 1 mA/cm^2 and 5 mA/cm^2. This strategy is generally applicable to Li metal anodes involving complex nanostructures. In addition, the dense and crystalline LiF coating improves the stability of Li_xSi NPs in both humid air and regular slurry solvent (NMP), indicating that LiF-Li_xSi NPs are potentially compatible with industrial electrode fabrication processes. With LiF coating, the decomposition of electrolytes is minimized to enable the consistently high CEs of LiF-Li_xSi NPs during long-term cycling (average CE of 99.92% from third cycle to 650th cycle). Therefore, this unique surface fluorination process brings huge benefit to both the existing Li-ion batteries and next-generation Li metal batteries. This fluorination method not only contributes significantly to the area of energy research but may also be applicable in other fields, such as graphene modification and organic synthesis.

■ ASSOCIATED CONTENT

Supporting Information

The Supporting Information is available free of charge on the ACS Publications website at DOI: 10.1021/jacs.7b05251.

Complete experimental details and additional characterizations, including supplemental Figures S1−S21 (PDF)

■ AUTHOR INFORMATION

Corresponding Author

*yicui@stanford.edu

ORCID

Jie Zhao: 0000-0001-6446-8313
Feifei Shi: 0000-0002-9171-6180
Ting Lei: 0000-0001-8190-9483
Allen Pei: 0000-0001-8930-2125
Jin Xie: 0000-0002-6270-1465
Yuzhang Li: 0000-0002-1502-7869
Zhenan Bao: 0000-0002-0972-1715

Author Contributions

⊥J.Z. and L.L. contributed equally to this work.

Notes

The authors declare no competing financial interest.

■ ACKNOWLEDGMENTS

We acknowledge the support from the Assistant Secretary for Energy Efficiency and Renewable Energy, Office of Vehicle Technologies, Battery Materials Research (BMR) and Battery 500 Program of the U.S. Department of Energy. A.P. acknowledges the support from the U.S. Department of Defense through the National Defense Science & Engineering Graduate Fellowship (NDSEG) Program and from Stanford University through the Stanford Graduate Fellowship (SGF) Program. We thank Dr. Hongwei Zhou, Dr. Hailin Peng, and Mr. Bing Deng for the discussion and help.

■ REFERENCES

(1) Lu, J.; Chen, Z.; Ma, Z.; Pan, F.; Curtiss, L. A.; Amine, K. *Nat. Nanotechnol.* **2016**, *11*, 1031−1038.
(2) Goodenough, J. B. *Acc. Chem. Res.* **2013**, *46*, 1053−1061.
(3) Larcher, D.; Tarascon, J. M. *Nat. Chem.* **2015**, *7*, 19−29.
(4) Sun, Y.; Liu, N.; Cui, Y. *Nat. Energy* **2016**, *1*, 16071.
(5) Scrosati, B.; Garche, J. *J. Power Sources* **2010**, *195*, 2419−2430.
(6) Xu, W.; Wang, J.; Ding, F.; Chen, X.; Nasybulin, E.; Zhang, Y.; Zhang, J.-G. *Energy Environ. Sci.* **2014**, *7*, 513−537.
(7) Aurbach, D.; Zinigrad, E.; Cohen, Y.; Teller, H. *Solid State Ionics* **2002**, *148*, 405−416.
(8) Obrovac, M. N.; Chevrier, V. L. *Chem. Rev.* **2014**, *114*, 11444−11502.
(9) Ko, M.; Chae, S.; Ma, J.; Kim, N.; Lee, H.-W.; Cui, Y.; Cho, J. *Nat. Energy* **2016**, *1*, 16113.
(10) Sathiya, M.; Rousse, G.; Ramesha, K.; Laisa, C. P.; Vezin, H.; Sougrati, M. T.; Doublet, M. L.; Foix, D.; Gonbeau, D.; Walker, W.; Prakash, A. S.; Ben Hassine, M.; Dupont, L.; Tarascon, J. M. *Nat. Mater.* **2013**, *12*, 827−835.
(11) Seo, D. H.; Lee, J.; Urban, A.; Malik, R.; Kang, S.; Ceder, G. *Nat. Chem.* **2016**, *8*, 692−697.
(12) Shen, C. F.; Ge, M. Y.; Zhang, A. Y.; Fang, X.; Liu, Y. H.; Rong, J. P.; Zhou, C. W. *Nano Energy* **2016**, *19*, 68−77.
(13) Ma, L.; Hendrickson, K. E.; Wei, S. Y.; Archer, L. A. *Nano Today* **2015**, *10*, 315−338.
(14) Aurbach, D.; McCloskey, B. D.; Nazar, L. F.; Bruce, P. G. *Nat. Energy* **2016**, *1*, 16128.
(15) Hassoun, J.; Jung, H.-G.; Lee, D.-J.; Park, J.-B.; Amine, K.; Sun, Y.-K.; Scrosati, B. *Nano Lett.* **2012**, *12*, 5775−5779.
(16) Tikekar, M. D.; Choudhury, S.; Tu, Z.; Archer, L. A. *Nat. Energy* **2016**, *1*, 16114.
(17) Zhao, J.; Zhou, G.; Yan, K.; Xie, J.; Li, Y.; Liao, L.; Jin, Y.; Liu, K.; Hsu, P. C.; Wang, J.; Cheng, H. M.; Cui, Y. *Nat. Nanotechnol.* **2017**, DOI: 10.1038/nnano.2017.129.
(18) Aurbach, D.; Weissman, I.; Schechter, A.; Cohen, H. *Langmuir* **1996**, *12*, 3991−4007.
(19) Xu, K. *Chem. Rev.* **2014**, *114*, 11503−11618.
(20) Bhattacharyya, R.; Key, B.; Chen, H.; Best, A. S.; Hollenkamp, A. F.; Grey, C. P. *Nat. Mater.* **2010**, *9*, 504−510.
(21) Li, W.; Yao, H.; Yan, K.; Zheng, G.; Liang, Z.; Chiang, Y.-M.; Cui, Y. *Nat. Commun.* **2015**, *6*, 7436.
(22) Lin, D. C.; Liu, Y. Y.; Liang, Z.; Lee, H. W.; Sun, J.; Wang, H. T.; Yan, K.; Xie, J.; Cui, Y. *Nat. Nanotechnol.* **2016**, *11*, 626−632.
(23) Liang, Z.; Lin, D. C.; Zhao, J.; Lu, Z. D.; Liu, Y. Y.; Liu, C.; Lu, Y. Y.; Wang, H. T.; Yan, K.; Tao, X. Y.; Cui, Y. *Proc. Natl. Acad. Sci. U. S. A.* **2016**, *113*, 2862−2867.
(24) Teyssot, A.; Belhomme, C.; Bouchet, R.; Rosso, M.; Lascaud, S.; Armand, M. *J. Electroanal. Chem.* **2005**, *584*, 70−74.
(25) Ding, F.; Xu, W.; Graff, G. L.; Zhang, J.; Sushko, M. L.; Chen, X.; Shao, Y.; Engelhard, M. H.; Nie, Z.; Xiao, J.; Liu, X.; Sushko, P. V.; Liu, J.; Zhang, J.-G. *J. Am. Chem. Soc.* **2013**, *135*, 4450−4456.
(26) Zheng, G.; Lee, S. W.; Liang, Z.; Lee, H.-W.; Yan, K.; Yao, H.; Wang, H.; Li, W.; Chu, S.; Cui, Y. *Nat. Nanotechnol.* **2014**, *9*, 618−623.
(27) Yan, K.; Lee, H.-W.; Gao, T.; Zheng, G.; Yao, H.; Wang, H.; Lu, Z.; Zhou, Y.; Liang, Z.; Liu, Z.; Chu, S.; Cui, Y. *Nano Lett.* **2014**, *14*, 6016−6022.
(28) Li, N. W.; Yin, Y. X.; Yang, C. P.; Guo, Y. G. *Adv. Mater.* **2016**, *28*, 1853−1858.
(29) Wu, M.; Wen, Z.; Liu, Y.; Wang, X.; Huang, L. *J. Power Sources* **2011**, *196*, 8091−8097.
(30) Kozen, A. C.; Lin, C.-F.; Pearse, A. J.; Schroeder, M. A.; Han, X.; Hu, L.; Lee, S.-B.; Rubloff, G. W.; Noked, M. *ACS Nano* **2015**, *9*, 5884−5892.
(31) Kazyak, E.; Wood, K. N.; Dasgupta, N. P. *Chem. Mater.* **2015**, *27*, 6457−6462.
(32) Jones, J.; Anouti, M.; Caillon-Caravanier, M.; Willmann, P.; Sizaret, P.-Y.; Lemordant, D. *Fluid Phase Equilib.* **2011**, *305*, 121−126.
(33) Dong, H.; Dorfman, S. M.; Holl, C. M.; Meng, Y.; Prakapenka, V. B.; He, D.; Duffy, T. S. *High Pressure Res.* **2014**, *34*, 39−48.
(34) Shiraishi, S.; Kanamura, K.; Takehara, Z.-i. *J. Electrochem. Soc.* **1999**, *146*, 1633−1639.
(35) Zhang, X. Q.; Cheng, X. B.; Chen, X.; Yan, C.; Zhang, Q. *Adv. Funct. Mater.* **2017**, *27*, 1605989.
(36) Michan, A. L.; Parimalam, B. S.; Leskes, M.; Kerber, R. N.; Yoon, T.; Grey, C. P.; Lucht, B. L. *Chem. Mater.* **2016**, *28*, 8149−8159.
(37) Heine, J.; Hilbig, P.; Qi, X.; Niehoff, P.; Winter, M.; Bieker, P. *J. Electrochem. Soc.* **2015**, *162*, 1094−1101.
(38) Lu, Y.; Tu, Z.; Archer, L. A. *Nat. Mater.* **2014**, *13*, 961−969.

DOI: 10.1021/jacs.7b05251
J. Am. Chem. Soc. XXXX, XXX, XXX−XXX

(39) Choudhury, S.; Archer, L. A. *Adv. Electron. Mater.* **2016**, *2*, 1500246.
(40) Stubblefield, C. B.; Bach, R. O. *J. Chem. Eng. Data* **1972**, *17*, 491−492.
(41) Ai, G.; Wang, Z. H.; Zhao, H.; Mao, W. F.; Fu, Y. B.; Yi, R.; Gao, Y.; Battaglia, V.; Wang, D. H.; Lopatin, S.; Liu, G. *J. Power Sources* **2016**, *309*, 33−41.
(42) Zhao, J.; Lu, Z.; Liu, N.; Lee, H.-W.; McDowell, M. T.; Cui, Y. *Nat. Commun.* **2014**, *5*, 5088.
(43) Zhao, J.; Lee, H.-W.; Sun, J.; Yan, K.; Liu, Y.; Liu, W.; Lu, Z.; Lin, D.; Zhou, G.; Cui, Y. *Proc. Natl. Acad. Sci. U. S. A.* **2016**, *113*, 7408−7413.
(44) Wang, L.; Fu, Y. B.; Battaglia, V. S.; Liu, G. *RSC Adv.* **2013**, *3*, 15022−15027.
(45) Zhao, J.; Lu, Z.; Wang, H.; Liu, W.; Lee, H.-W.; Yan, K.; Zhuo, D.; Lin, D.; Liu, N.; Cui, Y. *J. Am. Chem. Soc.* **2015**, *137*, 8372−8375.
(46) Lee, W. H.; Suk, J. W.; Chou, H.; Lee, J.; Hao, Y.; Wu, Y.; Piner, R.; Akinwande, D.; Kim, K. S.; Ruoff, R. S. *Nano Lett.* **2012**, *12*, 2374−2378.
(47) Aurbach, D.; Zaban, A. *J. Electroanal. Chem.* **1994**, *367*, 15−25.

DOI: 10.1021/jacs.7b05251
J. Am. Chem. Soc. XXXX, XXX, XXX−XXX